



1

Received 9 September 2025; revised; accepted; date of current version.

Digital Object Identifier 10.1109/JMW.20XX.0000000

Cryogenic RF MEMS Switch with Electronic Calibration Capability

Lafe F. Spietz¹, Chris Giovanniello², Brandon Takaki², Wei Ye³, Beverly Boiko⁴, Christian J. Long¹, Nathan E. Flowers-Jacobs¹, Adam J. Sirois¹, Peter F. Hopkins¹, Samuel P. Benz¹, Dylan Williams¹ (Life Fellow, IEEE)

¹National Institute of Standards and Technology, Boulder, CO 80305, USA ²Menlo Microsystems, Inc., Irvine, CA 92618-3768, USA ³ETLinx Systems, LLC, Chelmsford, MA 01824, USA ⁴ FormFactor, Boulder, CO 80301, USA

CORRESPONDING AUTHOR: D. Williams (e-mail: dylan@ieee.org).

ABSTRACT We characterize a radio-frequency micro-electro-mechanical-systems single-pole-six-throw switch designed for cryogenic operation to 10 GHz from room temperature to millikelvin temperatures. The switch contains an internal electronic calibration capability suitable for performing multiport vector and large-signal network analysis at room temperature and cryogenic temperatures. We demonstrate two calibration types, the first designed for measuring the scattering parameters of microwave devices connectorized with 3.5 mm coaxial connectors and the second for measuring the scattering parameters of microwave devices connectorized with Sub-Miniature version A (SMA) connectors.

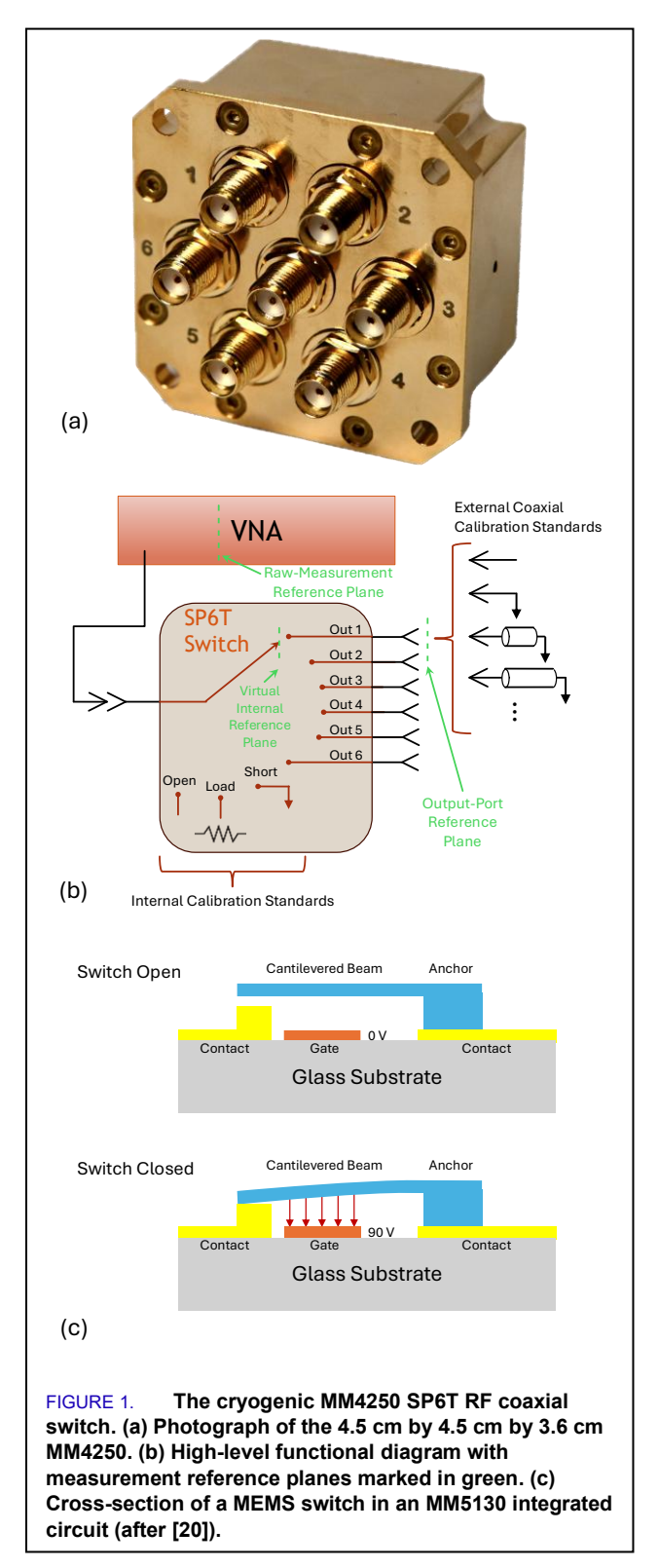
INDEX TERMS Cryogenic measurement, electronic calibration, micro-electro-mechanical-systems, radio frequency, vector network analysis.

I. INTRODUCTION

We describe the characterization and calibration of a coaxial radio-frequency (RF) micro-electro-mechanical-systems (MEMS) single-pole-six-throw (SP6T) switch to 10 GHz and from room temperature to millikelvin temperatures. We also calibrate and test an internal electronic calibration capability integrated into the switch that greatly simplifies calibrating vector network analyzers (VNAs) at the switch's output ports, especially at cryogenic temperatures. Finally, we develop two calibration types for the switch, the first designed for measuring the scattering parameters of devices under test (DUTs) connectorized with 3.5 mm coaxial connectors and the second for measuring the scattering parameters of DUTs connectorized with Sub-Miniature version A (SMA) connectors.

The first system for performing calibrated two-port vector scattering parameters at millikelvin temperatures was reported by Ranzani, et al., in [1]. Ranzani, et al. described a thru-reflect-line (TRL) calibration approach in coaxial transmission lines based on electromechanical coaxial switches. The switches route signals from the VNA through flexible coaxial cables to the coaxial TRL calibration standards and to a coaxial DUT. Ranzani, et al. applied their approach to the development and characterization of connectorized circuits in [2, 3]. Similar TRL calibration approaches suitable for use at millikelvin temperatures have been used by Yeh, et al. to characterize superconducting resonators [4], Oates, et al. [5] to characterize passive filters and a low noise amplifier, and others [6-8] to test coaxial cables, superconducting resonators, circulators and qubit drive-line components. More recently, Stanley and others [9-15] have taken a metrological approach to these measurements and established traceable coaxial calibrations based on the coaxial TRL calibration technique developed by Ranzani, et al., in [1] at millikelvin temperatures. Shin, et al. applied their coaxial switch system to perform calibrated measurements of Josephson traveling-wave parametric amplifiers in [13] and Stanley, et al. extended their approach to characterizing devices on printed circuit boards using flexible coaxial cables and electromechanical switches in [12, 14].

The first on-wafer measurement system for performing direct TRL calibrations and measurements on printed circuit boards and integrated circuits at millikely in temperatures was introduced by McEntee-Wei, et al. in [16]. This system, which is based on motorized positioners and commercial wafer probes, eliminates the need for switches and multiple electrically identical cables. Furthermore, the authors reported on the successful transfer of power and electrical phase measurements from room temperature to millikely in temperatures with this system, and applied it to the measurement of calibrated on-wafer scattering parameters, the characterization of interconnects between room-temperature and millikelvin reference planes, the calibrated measurement of microwave power and the calibrated measurement of modulated microwave signals of the type used to control qubits. Recent asyet-unreported work on this system has also greatly improved the repeatability and reliability of its positioners since the publication of [16]. However, this system is restricted to the characterization of devices on planar media.



However, all the approaches described above to performing calibrated scattering-parameter measurements in coaxial media still suffer from several deficiencies at cryogenic temperatures. They are based on electro-mechanical switches that are slow compared to many other technologies (including the switch we

¹ We use this term to mean less than 50 mK.





describe here), commonly generate electrical pulses at their outputs that can destroy sensitive low-noise amplifiers used in performing network analysis at millikelvin temperatures and Josephson-junction-based devices, and can generate enough heat to be significant at millikelvin temperatures (although some progress has been made to improve the switching efficiency of electro-mechanical switches at cryogenic temperatures [17], most heating seems to be due to the dissipation of mechanical energy in the switches). Also, they often use difficult-to-characterize flexible coaxial cables to connect thru-reflect-line (TRL) calibration standards and DUTs to the switch and rely on symmetry in the switches and flexible cables to obtain accurate calibrations.

In this work, we characterize and calibrate a Menlo Microsystems² MM4250 SP6T RF coaxial switch shown in Fig. 1a. The MM4250 is based on Menlo's Ideal Switch[®] technology, which is a MEMS process technology. The Ideal Switch[®] technology uses micromachined electrostatically controlled cantilevers to route RF signals with a 16 μs switching time and low energy dissipation. The MM4250 is designed to be a direct replacement for RF electro-mechanical switches currently in use at cryogenic temperatures.

The internal electronic calibration capability of the MM4250 switch greatly simplifies calibrations for the user. Unlike a standard electronic calibration unit [18, 19], which would calibrate a VNA to the switch's input port, we set the calibration reference planes in our experiments to the output ports of the switch. This allows use of the switch's internal electronic calibration standards to calibrate a VNA connected to the input port of the switch to any of the switch's six output ports over a wide range of temperatures with a calibration adapted to characterizing either 3.5 mm-connectorized DUTs or SMA-connectorized DUTs.

II. CRYOGENIC SP6T RF SWITCH

Figure 1 shows a photograph and high-level functional block diagram of the MM4250 RF switch that we characterized. The switch's SMA input port can be seen in Fig. 1a in the center of the switch face surrounded by its six SMA output ports near the periphery of the switch.

The MM4250 has a 3 dB bandwidth of approximately 8 GHz. The transmission coefficients of the six paths between the input port and the six output ports of the switch we tested had a standard deviation of less than ± 0.2 dB and ± 4 degrees over the switch's 8 GHz bandwidth.

The MM4250 is built using a series of Menlo Microsystems MM5130 SP4T RF MEMS integrated-circuit switches that were put into production on November 18, 2020 [20]. The MM5130 are based on small micromachined and electrostatically actuated cantilevered beams, as shown in the cross-sectional sketch in Fig. 1c. The electrostatic force applied to the cantilevered beam when a voltage of approximately 90 V is applied to the gate is enough to pull the cantilever beam down until it makes contact with the contact pad printed on the glass substrate, closing the switch [21,

22]. Additional information regarding switch operation can be found in [20-24].

The MM5130s are fabricated using a 14-layer glass-based integrated-circuit fabrication technology. The switches themselves are fabricated on a glass substrate, as shown in the cross-sectional sketch in Fig. 1c. The individual switches are only about 50 µm by 50 µm in size and multiple switches are usually fabricated on each die. The low-resistance contacts are rated for billions of operations. Finally, a micromachined glass cover with through vias is bonded on top of each die to compete the assembly, which, after dicing, is then ready to be soldered to a printed circuit board. Some additional fabrication information can be found in [20].

Typical controllers used with the MM5130 are described in [20] and [24]. However, in these experiments we used a soon-to-be-commercially-available controller under development at Menlo Microsystems that is optimized for the standard 25 pin Micro-D connectors and wiring installed in BlueFors Dilution Refrigerators and used in the MM4250 SP6T switches we tested.

To construct a single MM4250 SP6T switch, nine MM5130 die are soldered on a multilevel printed circuit board and arranged in three levels. The first level of the SP6T switch design consists of a single MM5130 MEMS integrated circuit, which is used to select between either a) a set of internally selectable open, short and load calibration standards or b) allowing the signal to pass through to the second switching level, which selects between the main RF measurement paths.

The second-level SP4T switches fan out to the six output paths. The design employs a special triple-throw mode of the SP4T switches called the "super-port mode", which greatly improves return loss and insertion loss for applications requiring many cascaded switches [21]. Finally, for the third level, another set of switches are employed in the super-port mode for the purpose of increasing the channel to channel and off-state isolation to over 50 dB across the usable bandwidth, which is critical for making sensitive RF measurements at cryogenic temperatures.

Another key attribute of RF MEMS switches that makes them particularly useful for use in cryogenic applications is the extremely low joule-heating created during the switching operation. Typically, with RF MEMS switches, the closing operation is accomplished with the application of an electrostatic force to a micromachined cantilevered beam to close the circuit, which dissipates very little energy. In the case of the MM4250, we found that we could open and close the three levels of switches needed to connect an individual throw on the device at a rate of 5 kHz without changing the 25 mK base temperature in our dilution refrigerator by more than 2 mK [25]. As a result, there is no need to wait for the dilution refrigerator to cool-down after switching, as was required in [1], drastically increasing the number of measurements which can be performed in a given timeframe.

3

² We use brand names only to clarify the experimental configuration. The National Institute of Standards and Technology does not endorse commercial products. Other products may work as well or better.

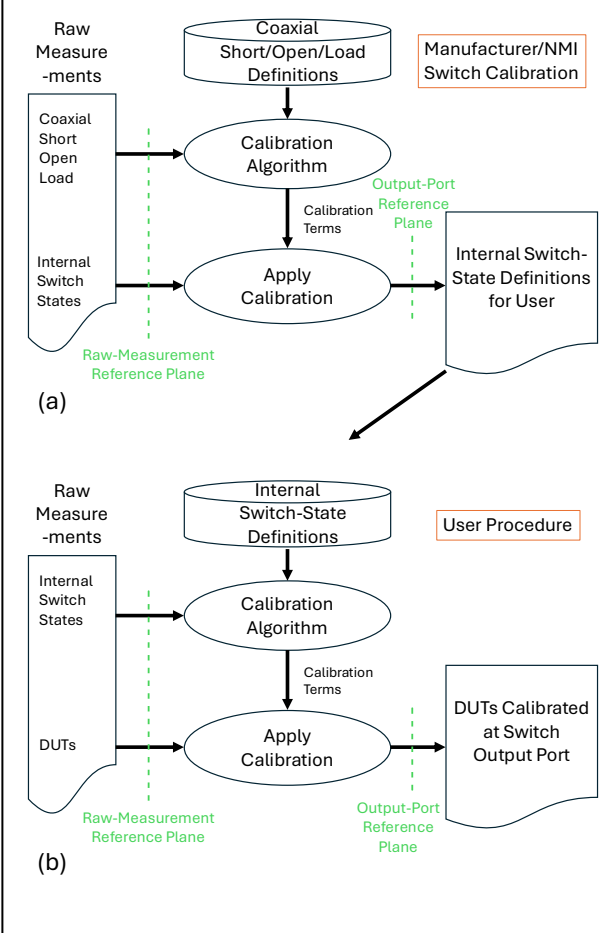


FIGURE 2. Coaxial switch calibration and application.
(a) Manufacturer or NMI calibrates switch. (b) User applies switch to calibrate DUTs at switch output port. The calibration reference-plane locations marked in green in this figure correspond to the physical reference-plane locations shown in green in Fig. 1b.

III. ROOM-TEMPERATURE CALIBRATION

Our ultimate goal is to calibrate the MM4250 switch for use at both room temperature and cryogenic environments. We start with a conventional room-temperature calibration to calibrate the switch's internal open, short and load states using a manufacturer-supplied 3.5 mm calibration kit and illustrate the calibration procedure without introducing complications encountered at lower temperatures. While we analyzed our measurements with the NIST Microwave Uncertainty Framework (MUF) [26], this room-temperature procedure is quite straight forward and could have been accomplished with a manufacturer-supplied 3.5 mm calibration kit and the built-in software of a standard VNA.

Electronic calibration units are typically used to reproduce a calibration at the end of a cable connected to a VNA [18, 19]. The calibration electronic calibration unit is straightforward. First, the manufacturer or a national metrology institute (NMI) calibrates a VNA at the end of a cable in their laboratory and connects that cable to the input of an electronic calibration unit. Then, the manufacturer or NMI measures the reflection coefficients of the internal states of the electronic calibration unit at a reference

plane at the end of the cable, which coincides with the input port of the electronic calibration unit.

Later, the user can reproduce the manufacturer's calibration, which is often traceable, in their laboratory at the end of a cable attached to their VNA simply by 1) connecting the electronic calibration unit to the cable on their VNA and 2) using the manufacturer or NMI calibrated measurements of the internal states of the electronic calibration unit as definitions for the user's measurements of those same internal states in their laboratory to calibrate the VNA. Now, the user's VNA is calibrated to a reference plane at the end of the cable that they attached to the electronic calibration unit provided by the manufacturer or NMI.

However, in our use case, the user of the MM4250 coaxial switch will typically want to connect the switch to the VNA and perform calibrated measurements at the output ports of the switch. Then the user will be able to measure up to six DUTs at a time in inaccessible locations due to cryogenic temperatures and vacuum enclosures. To address this use case, we calibrated the switch at its output ports, rather than its input port, before measuring the internal open, short and load states of the switch. The procedure we used in our dry run is shown in Fig. 2a and consisted of the following steps:

- 1. First, we connected our VNA to the input of the Menlo switch and set the switch to route signals from its SMA input port to its first SMA output port (labeled "Output-Port Reference Plane" in Fig. 2a), where we connected, one at a time, a coaxial open, short and load in a manufacturer-supplied calibration kit.
- 2. We then measured the internal open, short and load states of the switch.
- 3. We then repeated this procedure for the other five output ports of the switch.
- 4. Finally, using the MUF, we performed a calibration to a reference plane at each output port of the switch and applied that calibration to the internal open, short and load states measured at that same output port.

In practice, the measurements of the internal open, short and load states of the switch, with each set calibrated to a different output port of the switch, are all that users need to recalibrate their VNA to any one of the output ports of the switch. This "user procedure" is illustrated in Fig. 2b and can easily be performed with the built-in software of a standard VNA.

- 1. The user connects their VNA to the input port of the switch.
- 2. The user selects a calibration on their VNA that uses open, short and load definitions set equal to the measurements of the internal open, short and load switch states calibrated by the manufacturer or NMI with the procedure described above or in Section IV C at the desired output port of the switch.
- 3. The user then follows the prompts from the built-in VNA calibration software, selecting and measuring the switch's internal open, short and load states. The VNA software will now calibrate the user's VNA to the desired output port of the switch (labeled "Output-Port Reference Plane" in Fig. 2b).





The user procedure can be thought of as forcing the calibration on the user's VNA to map the internal states of the switch it measures to those that were recorded earlier when the manufacturer's or NMI's VNA was calibrated at a reference plane located at the desired output port of the switch. Because a one-port calibration is uniquely defined by three one-port calibration standards, this, in turn, forces the VNA to replicate measurements corrected by the earlier calibration when the switch was calibrated at that output port of the switch.

IV. CRYOGENIC CALIBRATION

Cryogenic calibration of the MM4250 presents several challenges. First, robust coaxial calibration standards must be modeled at both room temperature and cryogenic temperatures. Second, because we can only access the switches between cooldowns, we must develop a procedure that allows all calibration standards to be tested on each port while minimizing the impact of drift, cable bending and other changes in the setup between cooldowns. Finally, to improve accuracy, we try to avoid connecting our calibration standards to the switch with flexible cables, which are difficult to characterize at cryogenic temperatures. We now describe how we addressed these concerns.

A. Calibration Standards

For cryogenic calibrations, we used 3.5 mm offset shorts and a 3.5 mm offset open fabricated by Maury Microwave. The calibrations standards consisted of a 360B 834047 flat short, an 8047F6 833986 offset short of length 5.00 mm, an 8047P1.08 834105 offset short of length 10.08 mm, an 8047P1.8 834106 of length 18 mm, an 8047A6 816648 offset short of length 29.98 mm, and an 8048B6 838985 offset open of equivalent length 5.23 mm.

These gold-plated beryllium-copper offset shorts and an offset open offer a straightforward traceability path via dimensional measurements and circumvent the need to characterize dielectrics and use EM simulations used by Shokrolahzade, et al. [27]. These calibration standards also eliminate the need to connect them to the switch with difficult-to-characterize cables, as is usually done during cryogenic TRL calibrations, which are particularly sensitive to errors caused by cable repeatability and other small hardware inconsistencies. Then, in the strategy we adopted, later in the measurement process any cables that must be de-embedded from measurements can be characterized directly with a two-port switch calibration based on an "unknown" thru [28], which is less sensitive to repeatability and other hardware inconsistencies.

To assess accuracy at cryogenic temperatures and allow the use of the standards at low frequencies, we built temperature-dependent models of our calibration standards in the MUF using the dimensions and other quantities listed in Table 1. Given that the calibration standards were all built by the same manufacturer using the same materials and processes, we assumed the same material properties for all of them. Finally, we verified the models at room temperature with traceable sliding-load calibrations. Because we used physical models, they extend well to DC and could also be used with an uncharacterized auxiliary load and a one-port analogy of the calibration method described in [29] to

extend the scattering-parameter calibrations to very low frequencies.

We estimated the effective conductivity of the gold-plated beryllium-copper calibration standards from measurements of the electrical loss of the longest offset short with a calibrated VNA. As explained in note c of Table 1, we constrained the range by which we expected the effective electrical conductivity of the calibration standards to increase to a factor between 2 and 10 below 4 K, where we expect the electrical conductivity to be flat [30-32]. However, the conductivity of these calibration standards is quite high and the corresponding electrical loss so low that even this very large range of conductivities has little impact on the overall uncertainty evaluation we performed.

We used NIST Monograph 177 [32] to estimate the fractional change in the length of the calibration standards with temperature. Finally, we evaluated uncertainty due to repeatability, drift, and imperfect calibration-standard definitions using the regression residuals in the overdetermined offset-short/open calibration with the methods described in [33, 34], which are supported by the MUF.

TABLE 1. Calibration-Standard Characteristics

Quantity	Value	Standard Uncertainty
Inner-conductor diameter (mm)	1.52	0.006
Outer-conductor diameter (mm)	3.5	0.006
Outer-conductor lengths (mm)	-	0.015
Conductor eccentricity (mm)	0	0.06
Pin diameter (mm)	0.9	0.12
Pin-depth gap (mm)	0.045	0.018
Temperature coefficient of expansion ^a	-	-
Gold conductivity 295 K (S/M) ^b	1.2×10^7	0.5×10^7
Gold conductivity 4 K (S/M) ^c	7.2×10^7	2.8×10^7
Offset-open equivalent length (mm) ^b	5.23	0.015
Excess outer-conductor discontinuity capacitance (pF) ^d	0.009	0.0026

Values and standard uncertainties in this table were provided by the manufacturer unless otherwise noted.

^aFor Beryllium Copper C17300 M25 Alloy from formula 14-4 on page 14-8 of NIST Monograph 177 [32].

^bEstimated from room-temperature measurements performed with calibrated VNA.

^cWe estimated the effective metal conductivity to increase by a factor of 2 to 10 with rectangular distribution based on [30, 31]. Estimating the effective conductivity of the calibration standards low temperatures was complicated by skin-depth considerations and the fact that the electrical conductivity of thick pure plated gold can have a "residual resistivity ratio" (RRR), the ratio of room-temperature and 4 K resistivities, of up to 100 [30]. However, the manufacturer specified that the beryllium-copper calibration standards were plated with a 0.125 µm to 0.25 µm thick copper layer per AMS2418 followed by a 0.25 µm to 0.50 μm thick gold layer per MIL-DTL-45204, Type II, Grade D, Knoop Hardness 201 minimum. Based on the relatively thin 0.25 μm to 0.50 μm gold layer with only a 99.0 % minimum gold content and the discussions in [30, 31], it seemed possible that the conductivity of the gold layer might only increase by a factor of two at cryogenic temperatures, which would be similar to the increase of the conductivity of the copper layer and underlying beryllium-copper, suggesting a minimum factor of two increase of the effective conductivity of calibration standard at 4 K. On the high end, the conductivity of the gold plate could conceivably increase by a factor of up to 10 at 4 K, despite its thickness and impurities [30, 31], leading to a reduction of the skin depth and a greater concentration current at microwave frequencies.

dStandard uncertainty of 0.0026 pF reflects the difficulty of reading the graph in Fig. 9 of [35].

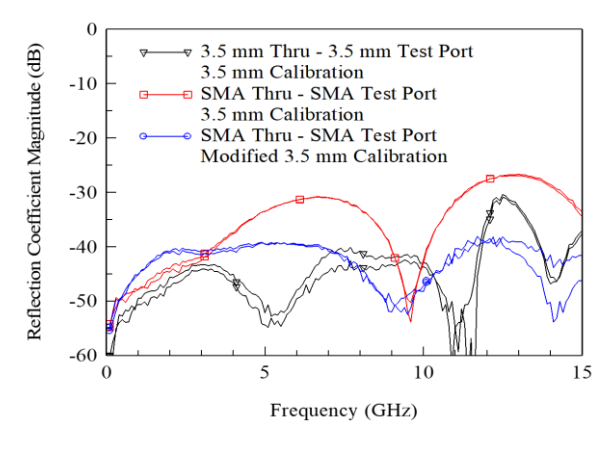


FIGURE 3. Comparison of two-port thru measurements performed with 3.5 mm and SMA test ports and corrected with 3.5 mm calibration and the modified 3.5 mm calibration adapted to SMA DUTs. Both S_{11} and S_{22} of each two-port measurement are plotted on the graph.³

B. 3.5 mm and SMA Calibration Reference Planes

Even though the MM4250 has SMA output ports and is physically compatible with both SMA-connectorized and 3.5 mm connectorized DUTs, our calibration kit is comprised of 3.5 mm calibration standards. As a result, our calibrations are, by design, most appropriate for characterizing 3.5 mm connectorized DUTs.

However, most users of the switch will be testing SMA-connectorized DUTs. To better accommodate these users, we developed a correction to the calibration to better adapt our calibration to SMA-connectorized DUTs. Following [35] and [36], we note that the primary difference between 3.5 mm male connectors on a user's DUT and the female SMA connectors on the switch is a step in the outer conductor of the SMA and 3.5 mm connectors, which can be modeled accurately in coaxial transmission lines as an excess shunt capacitance.

We used [35] to calculate the excess shunt capacitance of the step between the SMA and 3.5 mm connectors. From Fig. 7b of [35] and the standard internal dimensions of 3.5 mm and SMA connectors, $r_1 = 0.65$ mm, $r_2 = 1.75$ mm, $r_3 = 2.3$ mm, a = 1.1 mm, b = 1.65 mm, $\alpha = a/b = 0.67$, $r = r_3/r_1 = 3.54$ and $\varepsilon_r = 2.1$. From Fig. 9 of [35], the per-unit-length excess capacitance C'_{d2} due to the step in the outer conductors is approximately 0.0105 pF/cm and the total excess capacitance due to the step in the outer conductors C_d is, therefore, approximately 0.009 pF.

Based on this calculation and following [36], we were then able to augment our 3.5 mm calibration-standard definitions with a second set of modified calibration-standard definitions adapted for use with SMA-connectorized DUTs. This second set of modified calibration-standard definitions cancels the excess capacitance in the 3.5 mm calibration due to the step in the outer conductors formed when the 3.5 mm calibration standards are

³ The data in the plots in Figs. 3, 5 and 6 can be found at https://doi.org/10.18434/mds2-3967 and the GitHub repository https://github.com/lafefspietz/nist_MM4250_calibration_data_2025/.





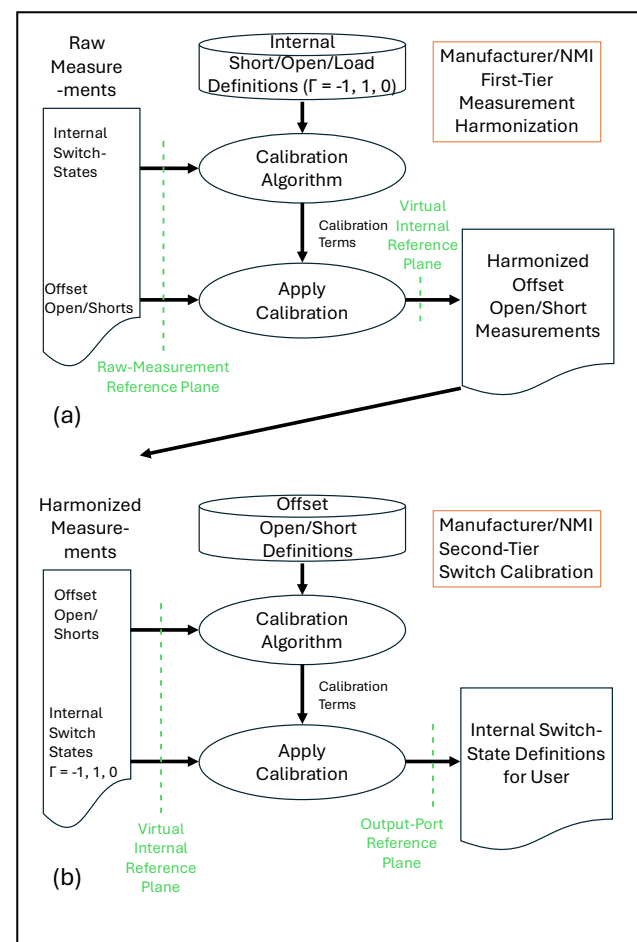


FIGURE 4. Manufacturer/NMI cryogenic coaxial switch calibration. (a) First-tier measurement harmonization. (b) Second-tier switch calibration. The calibration reference-plane locations marked in green in this figure correspond to the physical reference-plane locations shown in green in Fig. 1b.

connected to the SMA ports of the switch by incorporating a 0.009 pF capacitance into the 3.5 mm models of our calibration standards we use as standard definitions in the MUF.

We tested our new modified calibration definitions adapted for SMA-connectorized DUTs by performing a calibration on a VNA with female SMA test ports in our laboratory. We then calibrated the VNA with our 3.5 mm calibration kit and tested both a 3.5 mm thru and an SMA thru as DUTs. For comparison, we also calibrated a VNA with 3.5 mm test ports with our 3.5 mm calibration kit and used a 3.5 mm thru as a DUT.

Figure 3 compares the reflection coefficients of the 3.5 mm and SMA thrus we measured with our 3.5 mm calibration kit using the two test ports and calibration definitions. The measurements of the SMA thru shows that the new calibration definitions adapted for SMA measurements (blue marked with circles) significantly outperforms the conventional 3.5 mm calibration (red marked with squares) above 4 GHz and is comparable to the measurement of the 3.5 mm thru measured with a 3.5 mm calibration on a 3.5 mm test port (black marked with triangles).

C. Cryogenic Calibration Procedure

Calibrating the MM4250 at cryogenic temperatures with our calibration kit required six cooldowns, one for each calibration standard. We used a 0.5 W Gifford-McMahon 3 K cryocooler that cools much more quickly than the dilution refrigerators required to reach millikelvin temperatures and allowed us to achieve these six cooldowns in only about a week, rotating the calibration standards on the switch after each cooldown. Cable losses in this cryocooler were also low enough that we were able to simply run cables from the VNA ports directly through the cryocooler to the switch. However, we recognize that the wiring configurations used in [1] and [16] might improve our repeatability and reduce drift.

We expect every experimental setup to suffer in varying degrees from repeatability errors due to connection repeatability, VNA drift, cable drift and switch repeatability. With this in mind, we developed and tested an approach to harmonize the measurements we performed at each temperature during the six cooldowns to reduce VNA and cable drift at the expense of some increase in errors due to switch repeatability. We accomplished this with the procedure illustrated in Fig. 4 by using the internal open, short and load states in the switch itself to recalibrate the VNA to a constant "virtual" reference plane inside the switch to minimize the impact of repeatability, drift and temperature changes in the calibration process. Then, for each set of measurements at 295 K and 3 K, we measured the internal open, short and load states of the switch and the six calibration standards connected to the six output ports of the switch.

The procedure we used to analyze this data is illustrated in Fig. 4 and consisted of the following steps:

- As shown in Fig. 4a, after each temperature change, we used the measurements of the internal open, short and load states of the switch to perform a virtual first-tier calibration at our virtual internal reference plane (labeled in green in Fig. 4a) inside the switch. We then used this virtual calibration to correct the measurements of the calibration standards on each of the six output ports of the switch in that set. This virtual calibration simply defined the internal open, short and load states of the switch as ideal (i.e. a reflection coefficient of 1 for the open, -1 for the short and 0 for the load). This virtual first tier calibration corrects both the offset standards and the internal SOL, aligning all measurements to a new common reference plane that minimizes drift and other changes in the VNA and cables during the measurements. The second-tier calibration then uses these virtual drift-corrected offset standards, so that the internal short, open and load definitions that the user receives are also drift corrected.
- 2. Using these virtually calibrated first-tier measurements of our six calibration standards at one of the outputs of the switch, we performed a second-tier calibration illustrated in Fig. 4b at each temperature and switch output port.

3. Finally, we used this second-tier calibration to calibrate the now ideal⁴ virtually calibrated internal open, short and load measurements performed at that temperature and switch output port. These are now the internal open, short and load states of the switch calibrated at the output port of the switch that we were looking for and can be used directly in the user procedure of Fig. 2b.

D. Cryogenic Calibration Results

After performing two week-long sets of cooldowns and measuring each of the Maury calibration standards on each of the six ports on the MM4250, we calculated the switch's calibration coefficients and evaluated our measurement uncertainties. Figure 5 compares the uncertainty in the elements S_{21} , S_{11} and S_{22} of the two-port calibration error boxes of the switch determined by the second-tier calibration algorithm of Fig. 4b from the measurements performed at 295 K and 3 K. Curves labeled "Week 1" were taken during the first set of cooldowns, while curves labeled "Week 2" and "Week 2 Repeat" were taken during the second set of cooldowns.

The continuous brown curves marked with filled triangles in Fig. 5 show the systematic uncertainties we evaluated due to the uncertainty mechanisms listed in Table 1 of Section IV A. The total uncertainties of the elements of the error boxes at 295 K are shown in continuous red curves, while the uncertainties at 3 K are plotted in dashed blue lines. These curves add the uncertainty due to calibration residuals from the overdetermined offset open and offset shorts by the algorithm illustrated in Fig. 4b, which we evaluated using the methods described in [33, 34].

While our uncertainties are reasonable, the very small size of the systematic uncertainties plotted in continuous brown curves marked with filled triangles compared to the total uncertainties plotted in Fig. 5 indicates that repeatability errors of the cryogenic calibration performed over the six cool-down cycles dominated measurement uncertainties at both room temperature and cryogenic temperatures.

While difficult to see in the figures, our repeatability was significantly better during the measurement we performed at 295 K on week 1. This raises the possibility that we may be able to significantly lower our overall measurement uncertainty if we can identify and eliminate the sources of measurement repeatability errors in our experiments.

The cryogenic calibration we developed corrects for variations in the VNA and cables, and we can measure the actual temperature quite accurately. Furthermore, the repeatability errors shown in Fig. 5 are lower than those obtained when we applied the room-temperature calibration algorithm of Section III to our cryogenic data, as we would expect. So, we do not believe that variations in the VNA, cables or temperatures significantly impacted our measurement repeatability. However, factors that may have contributed to repeatability error during our experiments include the following:

1. SMA connectors generally have much lower repeatability than the precision 3.5 mm connectors on our calibration standards and are usually not considered suitable for precision metrology [37]. In particular, the

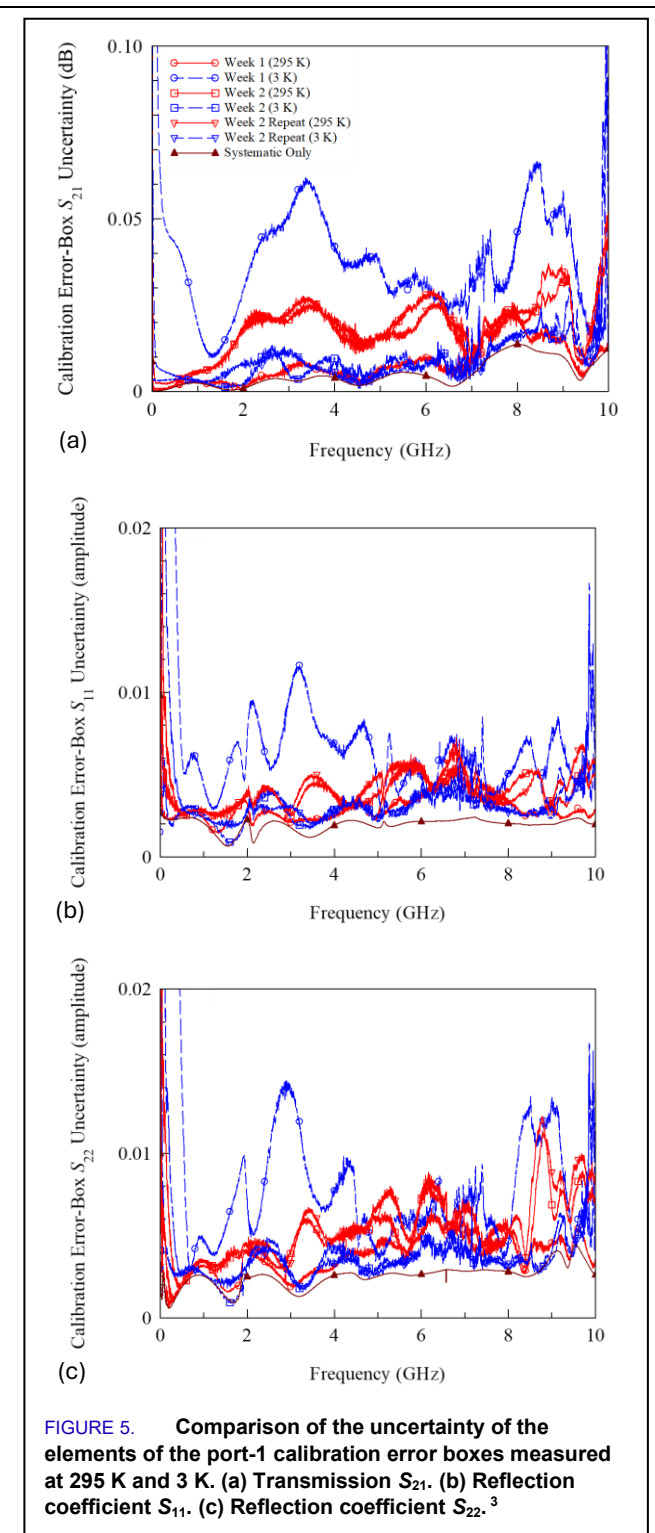
- outer conductors of our precision male 3.5 mm calibration standards are chamfered slightly where they mate with the thin mating surface on the SMA connectors used in the switches. Using precision 3.5 mm connectors on the switches would likely improve the repeatability of the connections to precision 3.5 mm calibration standards.
- 2. Degradation of repeatability at DC and RF in the underlying RF MEMS switches observed by Sorenson, et al. [38] and by Lee, et al. [39] at cryogenic temperatures. These observations could be related to mechanical stress, condensing gasses in the packaging and increased charge storage at cryogenic temperatures. It is likely that averaging repeated measurements performed during each cooldown would reduce these errors.

8

⁴ The virtually calibrated internal switch states are now ideal because we used ideal open, short and load definitions for those states in the virtual calibration described in the prior step. This calibration maps the internal measured states







V. MILLIKELVIN MEASUREMENTS

We tested the user procedure discussed in Section III and illustrated in Fig. 2b with a single cooldown in a dilution refrigerator on the same switch that we previously characterized in our fast-cooling 3 K cryostat in Section IV. This refrigerator was equipped with a VNA manufactured by a different vendor, discrete attenuators on the drive lines located at various

temperature stated of the refrigerator, cryogenic amplifiers for the reflected signals and an external 0.3 GHz - 14 GHz coupler located on the mixing chamber in a way similar to that described in [1] and shown in Fig. 2 of [16]. This results in approximately - 52 dBm of power at the DUT, which reduces noise in the measurements without appreciably impacting the base temperature of the refrigerator.

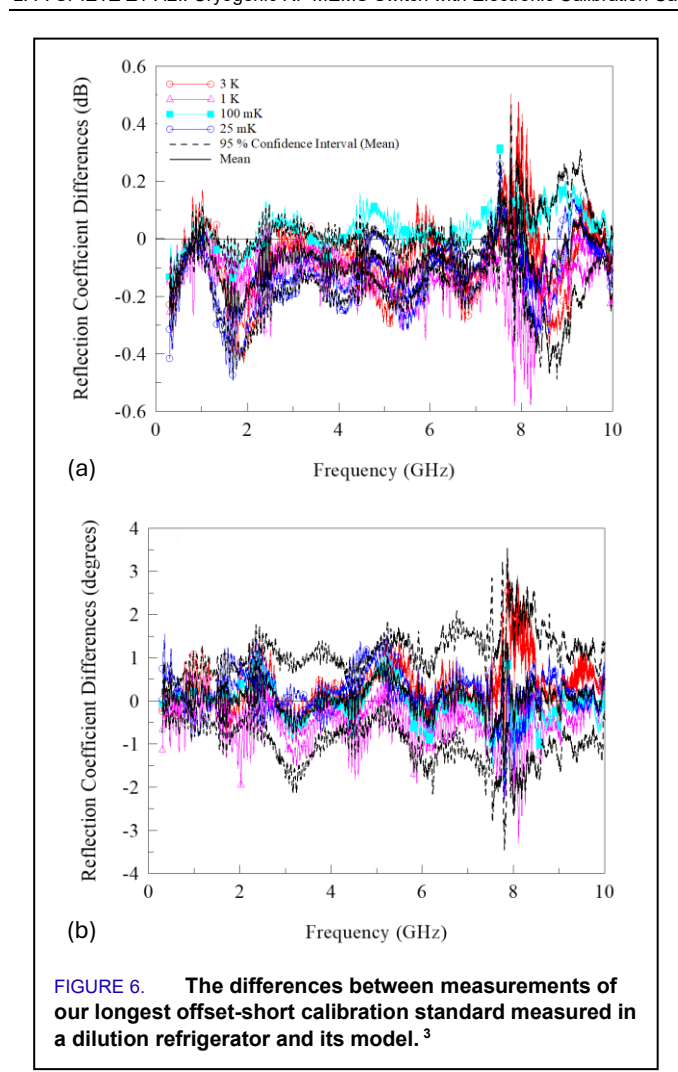
As the cool down progressed, we used the internal open, short and load states of the MM4250 to calibrate the VNA to the six output ports of the switch and perform measurements at each of those ports when the temperature on the mixing chamber reached 3 K, 1 K, 100 mK and 25 mK. We used our offset-shorts and offset-open calibration standards as DUTs in the test, with one calibration standard connected to each port. This was convenient, as we could compare our measurements to the offset-short models we developed in Section IV A.

Duplicating the user procedure illustrated in Fig. 2b, we first calibrated the VNA at 3 K, 1 K, 100 mK and 25 mK at each of the switch's output ports using the internal switch state definitions that we developed in our fast-turnaround 3 K cryostat and measured the DUTs connected on each port of the switch in the dilution refrigerator. Our 29.98 mm offset short was connected to the fourth output port of the switch, and we chose this calibration standard to illustrate the calibration capability of the switch because this offset short sweeps more quickly around the Smith Chart than the other calibration standards that we had available to us. We felt this would better validate our one-port measurements and calibrations, much as some use long Beatty standards [40] to test two-port calibrations.

Fig. 6 plots the differences between the reflection-coefficient measurements of our 29.98 mm offset short and the reflection coefficients of the model of the offset short we developed in colored lines with markers to indicate the temperature at which the measurement was performed. The differences we plot do not appear to drift in a systematic way with temperature, indicating that the 3 K internal switch state definitions we developed are appropriate for measurements at millikelvin temperatures. The errors at low frequencies are likely due to our calibration based on offset shorts and an offset open degrading as the locations of the offset shorts on the Smith Chart collapse and become degenerate near DC and no longer provide two of the three distinct calibration standards required to define a one-port calibration.

We also formed the mean of the measured differences shown in Fig. 6 and evaluated the uncertainty in this mean with the method proposed in [41], which has been incorporated into the MUF. Thus, the uncertainty we evaluated in the mean included the systematic errors in our offset-shorts and offset-open calibration standards we evaluated in Section IV A, the repeatability errors in the measurements of the switch's internal short, open and load states we discussed in Section IV D and the variation of the measured differences shown in Fig. 6 when we formed their mean, which were evaluated using the method of [41].

We then superimposed the mean of the measured differences in a solid black line and the 95 % confidence intervals we evaluated on that mean in dashed black lines on the plots in Fig. 6. In general, the differences we measured between the offset



short's measured and modeled reflection coefficients fell within the 95 % confidence intervals we evaluated. However, the average and its uncertainty in Fig. 6a do reveal what appears to be a tenth of a decibel of systematic error in the magnitude of our measurements in the dilution refrigerator. Fig. 6b does not seem to indicate any statistically significant systematic differences in phases of the reflection coefficients. We note that the uncertainties shown in Fig. 6 would have increased significantly if we had invoked assumptions of switch symmetry in our calibration process given the roughly ± 0.2 dB and ± 4 degrees standard deviations of the transmission coefficients of the six paths through the switch we measured at the high end of the switch's 8 GHz bandwidth.

VI. CONCLUSION

Our results illustrate the ability of the internal switch states of the Menlo Systems MM4250 coaxial SP6T switch to calibrate VNAs and evaluate the uncertainties in the measurements we make at cryogenic temperatures. Users need only select a calibration kit on their VNA for the desired switch port and temperature and follow the VNA calibration prompts while selecting the correct internal state of the switch. Furthermore, if

the manufacturer or NMI provided traceable definitions, the user's calibration could be made traceable as well.

We used precision offset shorts and an offset open that are straightforward to model and do not require the use of flexible cables on the switch's output ports, simplifying traceability. For calibrations at cryogenic temperatures, we introduced a novel measurement harmonization approach that improves calibration quality by correcting measurements to a uniform virtual reference plane, which minimizes drift and repeatability errors across multiple cooldowns. We also note that errors due to imperfect switch repeatability might be further reduced by averaging repeated measurements performed during each cooldown.

We also described a novel method for adapting the native 3.5 mm calibrations we started with to the characterization of DUTs with standard SMA connectors, improving accuracy for SMA-connectorized devices. Notably, by performing separate calibrations on each port, we do not need to invoke *any* assumptions of symmetry in the switch. All these approaches could be implemented with electro-mechanical switches as well.

We found that the measurement uncertainties were dominated by repeatability. The role that repeatability plays in the measurements emphasizes the importance of evaluating the uncertainty due to repeatability, which we evaluated using the methods of [33, 34, 41].

In closing, we note that the one-port internal calibration capability of these switches can be extended to multiport calibrations using reciprocal thru standards [28]. This not only allows for the characterization of multiport devices, but also for the characterization of various adapters and cables that can then be used to accurately move the switch's measurement reference planes in complex measurement systems and experiments and for the direct characterization and calibration of uncalibrated switches at cryogenic temperatures. The switches can also be used to support large-signal calibrations with calibrated amplitude and phase at cryogenic temperatures using the methods described in [16]. Also, because our physical calibration models extend well to low frequencies and the switches continue to operate well at DC, our calibration models can be used to characterize sets of auxiliary loads following the calibration method described in [29]. Then, following [29], these auxiliary loads combined with our offset open and shortest offset short could be used to build broad-band cryogenic short-open-load calibration kits for use at any frequency from DC to the highest frequencies supported by the switch at both room temperature and cryogenic temperatures.

In addition, the MM4250 comes with internal open, short and load states that can be connected to its six output ports.⁵ Characterizing these states and the paths through an MM4250 will greatly simplify the calibrated measurement of noise parameters. The internal open, short and load states at the output ports of an MM4250 can also be used to streamline the transfer of calibrations from one switch to another.

Finally, as production of RF MEMS switches currently under development ramps up, we expect that switches supporting frequencies of 30 GHz or higher and with much higher throw counts will soon become available. We expect that these advances in manufacturing, combined with the advances in calibration and

DUT on the same output port, and thus cannot replace the functionality of the internal states on the switch's input port.

⁵ Due to limitations on the number of control lines used by the switch, the internal states on the output port of the switch cannot be disconnected from the





measurement techniques we demonstrated in this paper, will provide the quantum-computing industry with a formidable RF toolkit adapted to the inaccessible cryogenic environments they depend on. This RF toolkit will allow for traceable turnkey RF large-signal scattering-parameter, and noise-parameter measurements directly in their laboratories for characterization of multiport RF components, room-temperatureto-cryogenic-temperature interconnects, modulated signals, nonlinear devices and cryogenic semiconductor superconducting amplifiers.

ACKNOWLEDGMENT

We thank Joe Aumentado at NIST for his guidance and support of this work, Angela Stelson at NIST for her assistance with performing accurate room temperature measurements, Li-Anne Liew at NIST for her advice on operating these switches at cryogenic temperatures, Aric Sanders at NIST for useful guidance with Python and calibrations, Steve Waltmann at Google Quantum AI for useful discussions concerning RF circuits, and Dan Schmidt at NIST and Jacob Alldredge at JHU/APL for useful discussions about the conductivity of plated gold.

REFERENCES

- [1] L. Ranzani, L. Spietz, Z. Popovic, and J. Aumentado, "Two-port microwave calibration at millikelvin temperatures," *Review of Scientific Instruments*, vol. 84, no. 3, p. 034704, 2013/03/01 2013, doi: 10.1063/1.4794910.
- [2] L. Ranzani et al., "Wideband Isolation by Frequency Conversion in a Josephson-Junction Transmission Line," *Physical Review Applied*, vol. 8, no. 5, p. 054035, 11/17/2017, doi: 10.1103/PhysRevApplied.8.054035.
- [3] L. Ranzani, L. Spietz, and J. Aumentado, "Broadband calibrated scattering parameters characterization of a superconducting quantum interference device amplifier," *Applied Physics Letters*, vol. 103, no. 2, p. 022601, 2013/07/08 2013, doi: 10.1063/1.4813549.
- [4] J.-H. Yeh and S. M. Anlage, "In situ broadband cryogenic calibration for two-port superconducting microwave resonators," *Review of Scientific Instruments*, vol. 84, no. 3, p. 034706, 2013/03/01 2013, doi: 10.1063/1.4797461.
- [5] D. E. Oates, R. L. Slattery, and D. J. Hover, "Cryogenic test fixture for two-port calibration at 4.2 K and above," in 2017 89th ARFTG Microwave Measurement Conference (ARFTG), 9–9 June 2017 2017, pp. 1–4, doi: 10.1109/ARFTG.2017.8000842.
- [6] C. R. H. McRae, "Measurement Techniques for Superconducting Microwave Resonators Towards Quantum Device Applications," in 2022 IEEE/MTT-S International Microwave Symposium - IMS 2022, 19–24 June 2022 2022, pp. 230–232, doi: 10.1109/IMS37962.2022.9865517.
- [7] S. Simbierowicz, V. Y. Monarkha, S. Singh, N. Messaoudi, P. Krantz, and R. E. Lake, "Microwave calibration of qubit drive line components at millikelvin temperatures," *Applied Physics Letters*, vol. 120, no. 5, p. 054004, 2022/01/31 2022, doi: 10.1063/5.0081861.
- [8] T. Arakawa and S. Kon, "Calibrated Two-Port Microwave Measurement up to 26.5 GHz for Wide Temperature Range From 4 to 300 K," *IEEE Transactions on Instrumentation and Measurement*, vol. 72, pp. 1–8, 2023, doi: 10.1109/TIM.2023.3315393.
- [9] M. Stanley et al., "A Technique to Improve Accuracy of S-Parameter Measurements of Coaxial Connectorized Devices at Cryogenic Temperatures," *IEEE Transactions on Instrumentation and Measurement*, vol. 74, pp. 1–12, 2025, doi: 10.1109/TIM.2025.3595257.
- [10] M. Celep, S. H. Shin, M. Stanley, E. Breakenridge, S. Singh, and N. Ridler, "SI Traceable RF and Microwave Power Measurements at Cryogenic Temperatures," in 2024 Conference on Precision Electromagnetic Measurements (CPEM), 8–12 July 2024 2024, pp. 1–2, doi: 10.1109/CPEM61406.2024.10646150.
- [11] S. H. Shin, M. Stanley, J. Skinner, S. E. d. Graaf, and N. M. Ridler, "Broadband Coaxial S-Parameter Measurements for Cryogenic Quantum Technologies," *IEEE Transactions on Microwave Theory and Techniques*, vol. 72, no. 4, pp. 2193–2201, 2024, doi: 10.1109/TMTT.2023.3322909.

- [12] M. Stanley et al., "RF and microwave metrology for quantum computing recent developments at the UK's National Physical Laboratory," International Journal of Microwave and Wireless Technologies, vol. 16, no. 4, pp. 535–543, 2024, doi: 10.1017/S1759078724000369.
- [13] S. H. Shin et al., "In-operando microwave scattering-parameter calibrated measurement of a Josephson traveling wave parametric amplifier," Applied Physics Letters, vol. 125, no. 10, p. 104001, 2024, doi: 10.1063/5.0220776.
- [14] M. Stanley, S. D. Graaf, T. Hönigl-Decrinis, T. Lindström, and N. M. Ridler, "Characterizing Scattering Parameters of Superconducting Quantum Integrated Circuits at Milli-Kelvin Temperatures," *IEEE Access*, vol. 10, pp. 43376–43386, 2022, doi: 10.1109/ACCESS.2022.3169787.
- [15] M. Stanley, R. Parker-Jervis, S. de Graaf, T. Lindström, J. E. Cunningham, and N. M. Ridler, "Validating S-parameter measurements of RF integrated circuits at milli-Kelvin temperatures," *Electronics Letters*, https://doi.org/10.1049/ell2.12545 vol. 58, no. 16, pp. 614–616, 2022/08/01 2022, doi: https://doi.org/10.1049/ell2.12545.
- [16] E. McEntee-Wei, R. A. Chamberlin, N. Kilmer, J. Kast, J. A. Connors, and D. Williams, "On-Wafer Vector-Network-Analyzer Measurements at mK Temperatures," *IEEE Journal of Microwaves*, pp. 1–12, 2023, doi: 10.1109/JMW.2022.3232076.
- [17] F. Janot, "Technology Guide for Cryogenic RF switches," Radiall, 2023.
 [Online]. Available:
 https://www.radiall.com/media/document_library/Technology_Guide_for_Cryogenic RF switches Rev 1.0.pdf
- [18] V. Adamian, "A Novel Procedure for Network Analyzer Calibration and Verification," in 41st ARFTG Conference Digest, 18–18 June 1993 1993, vol. 23, pp. 8–17, doi: 10.1109/ARFTG.1993.327013.
- [19] V. Adamian, "Simplified Vector Network Analyzer Design Using an Electronic Calibrator," in 45th ARFTG Conference Digest, 19–19 May 1995 1995, vol. 27, pp. 64–73, doi: 10.1109/ARFTG.1995.327107.
- [20] Menlo-Microsystems, "MM5130 Application Note v1.1," 2025. [Online]. Available: https://menlomicro.com/
- [21] Menlo-Microsystems, "Avoiding Floating Nodes in Ohmic MEMS Circuits - Application Note AN-0002 v1.1," 2022. [Online]. Available: https://menlomicro.com/
- [22] Menlo-Microsystems. "How it Works Ideal Switch for RF." https://menlomicro.com/technology/how-it-works (accessed 2025).
- [23] Menlo-Microsystems, "MM5130 DC to 26 GHz High Power RF Switch Datasheet ver 2.44," 2022. [Online]. Available: https://menlomicro.com/
- [24] Menlo-Microsystems. "Ideal Switch RF Switches." https://menlomicro.com/products/rf (accessed 2025).
- [25] B. Takaki and B. Boiko, "MM4250 Testing at Form Factor: Switch Module Functionality and Temperature Monitoring," Menlo Microsystems, Inc., Irvine, CA, Unpublished Report 2025.
- [26] NIST Microwave Uncertainty Framework. (2011). National Institute of Standards and Technology. [Online]. Available: http://www.nist.gov/ctl/rf-technology/related-software.cfm
- [27] E. Shokrolahzade et al., "Thermo-Mechanical EM Models for Broadband Cryogenic VNA Calibration Including Numerical Uncertainties Down to 4.2 K," *IEEE Transactions on Microwave Theory and Techniques*, pp. 1–12, 2025, doi: 10.1109/TMTT.2025.3584196.
- [28] A. Ferrero, "Two-port network analyzer calibration using an unknown 'thru'," *IEEE Microw. Guided Wave Lett.*, vol. 2, no. 12, pp. 505–507, 1992.
- [29] D. F. Williams and R. B. Marks, "LRM Probe-Tip Calibrations with Imperfect Resistors and Lossy Lines," in *Proc. ARFTG Microw. Meas. Conf.*, December 1993, vol. 42, pp. 32–36.
- [30] T. P. Bernat, N. B. Alexander, and J. L. Kaae, "Thermal and Electrical Conductivities of Electroplated Gold," *Fusion Science and Technology*, vol. 51, no. 4, pp. 782–785, 2007, doi: 10.13182/FST07-A1479.
- [31] K. Vonk, "Electrodeposition of Gold (Au) for Transition Edge Sensor ATHENA +," Bachelor, Technische Natuurkunde (HHS)/ Applied Physics, The Hague University of Applied Sciences, The Hague, Netherlands, 2015.
- [32] N. J. Simon, E. S. Drexler, and R. P. Reed, "NIST Monograph 177 -Properties of Copper and Copper Alloys at Cryogenic Temperatures," National Institute of Standards and Technology, Washington, DC, 1992.
- [33] D. Williams, B. Jamroz, and J. Rezac, "Evaluating Uncertainty of Nonlinear Microwave Calibration Models with Regression Residuals," *IEEE Trans. Microw. Theory Techn.*, vol. 68, no. 9, pp. 3776 – 3782, 2020, doi: 10.1109/TMTT.2020.3005170.
- [34] D. Williams, B. F. Jamroz, J. Rezac, and R. Jones, "Evaluating Uncertainty of Microwave Calibrations with Regression Residuals," *IEEE Trans. Microw. Theory Techn.*, 2020, doi: 10.1109/TMTT.2020.2983358.

- [35] J. R. Whinnery, H. W. Jamieson, and T. E. Robbins, "Coaxial-Line Discontinuities," *Proceedings of the IRE*, vol. 32, no. 11, pp. 695–709, 1944, doi: 10.1109/JRPROC.1944.234027.
- [36] D. F. Williams, "Rectangular-waveguide vector-network-analyzer calibrations with imperfect test ports," in ARFTG Microw. Meas. Conf., December 2010, vol. 76, pp. 1–8.
- [37] D. Skinner, "Guidance on using Precision Coaxial Connectors in Measurement v3," 2007. [Online]. Available: http://resource.npl.co.uk/docs/networks/anamet/connector_guide_v3.pdf
- [38] E. Sorenson, P. Bradley, D. Lauria, and L. A. Liew, "A methodology for evaluating MEMS switch reliability at cryogenic temperatures," in *Proc.* Cryogenic Engineering Conference/International Cryogenic Materials Conference (CEC-ICMC 2025), Reno, NV (submitted), May 18–22, 2025.
- [39] Y. B. Lee, C. Devitt, X. Zhu, N. Yost, Y. Gu, and S. A. Bhave, "Cryogenic Performance Evaluation of Commercial SP4T Microelectromechanical Switch for Quantum Computing Applications," arXiv, 2025, doi: https://doi.org/10.48550/arXiv.2507.13574.
- [40] R. W. Beatty, "2-Port Quarter-Wavelength Waveguide Standard of Voltage Standing-Wave Ratio," *Electronics Letters*, vol. 9, no. 2, 1973. [Online]. Available: https://digital-library.theiet.org/doi/epdf/10.1049/el%3A19730017.
- [41] M. J. Frey, B. F. Jamroz, A. A. Koepke, J. D. Rezac, and D. Williams, "Monte-Carlo Sampling Bias in the Microwave Uncertainty Framework," *Metrologia*, vol. 56, no. 5, p. 13, 2019, doi: 10.1088/1681-7575/ab2c18.



LAFE SPIETZ received a BA degree from the University of California, Berkeley with a math physics double major in 1998. He completed a Ph.D. in applied physics at Yale University in 2006, where his dissertation research was building a novel low temperature thermometer based on the noise from a tunnel junction. He then joined the Applied Microwave Photonics group at NIST, where he designed and

built ultra-low noise microwave amplifiers using superconducting electronics. After a 12-year hiatus in the private sector, he has rejoined NIST in the superconductive electronics group, building microwave calibration and testing systems for use in the quantum information community using MEMS switches.



CHRIS GIOVANNIELLO, Co-Founder Menlo Micro & SVP RF Business Unit, is a seasoned technology executive with over three decades of experience driving innovation and growth across the semiconductor industry. Chris leads the strategy and development of cutting-edge RF solutions, playing a pivotal role in redefining the performance of next-generation electronic switching.

Before co-founding Menlo Micro, Chris served as VP Business Development at GE Ventures. He focused on monetization strategies across semiconductor, MEMS, and thermal management programs—via licensing, joint ventures, and strategic partnerships.

Prior to GE, Chris held a variety of senior leadership roles at Teradyne, global leader in ATE. He was responsible for launching a new services business and led large technical teams across Europe and the US. Chris also played a central role in defining and delivering new products for the ATE industry.

With a proven track record of building high-performance teams, scaling technology businesses, and delivering customer-centric innovation, Chris continues to be a driving force behind Menlo Micro's mission to revolutionize the world of electronic switching.



BRANDON TAKAKI is an Applications and Software Engineer at Menlo Microsystems, where he has contributed since 2021. In this role, he develops automated test systems for RF and power switch characterization, designs and programs embedded firmware for relay control systems and builds data analytics platforms. He received his B.S. in Computer Science and Engineering from the University of California. Irvine.



WEI YE received the B.S. degree in Electrical Engineering from the University of Electronic Science and Technology of China and the M.S. degree in Electrical Engineering (Radar and RF Communications) from the University of Connecticut, Storrs, CT, USA. He has over 40 years of experience in engineering design and management, specializing in RF and digital communication systems.

He is credited with over 11 U.S. patents in computing and signal processing and has been a key contributor in three successful startup acquisitions. He is currently President of ETLinx Systems, LLC, Chelmsford, MA, where he has served as an RF/Microwave Consulting Engineer since 2006, developing high-performance communication systems and ICs for commercial and defense clients.

Previously, he held senior engineering leadership roles at Narad Networks (acquired by Ciena) and Maxcomm Technologies (acquired by Cisco), and also served at Cisco Systems, Inc., as Senior Hardware Engineering Manager contributing to modem development and system integration. His technical expertise spans RF/microwave circuit design, communication system architectures and Microwave MCM/SIP module design.



BEVERLY N. BOIKO received her B.S./M.S. degree in Mechanical Engineering from the University of Colorado in Boulder, Colorado, USA in 2017. From 2015 to 2020 she worked as a Cryogenic Mechanical Engineer at High Precision Devices Inc. where she designed low temperature systems used for astronomy, condensed matter physics, and high-performance computing. Since Fall of 2020, she has worked as Sr. Principal Application Engineer at FormFactor

inc. in Boulder, Colorado, USA, where she is focused on developing the quantum applications for the HPD cryogenics product group. She also established the Advanced Cryogenic Lab to enable cryogenic testing as a service within the quantum supply chain.



CHRISTIAN J. LONG received the B.S. and Ph.D. degrees in physics from the University of Maryland at College Park, College Park, MD, USA, in 2004 and 2011, respectively. His doctoral research focused on the development of both microwave near-field scanning probe microscopy techniques and new methods to analyze data from combinatorial materials experiments. From 2012 to 2015 he was a postdoctoral research fellow with the National

Institute of Standards and Technology (NIST), Gaithersburg, USA, where he focused on techniques for characterizing nanoscale materials. In 2016, he joined the staff at NIST, Boulder, USA, to work on development of standards for microwave and mm-wave calibrations.







NATHAN E. FLOWERS-JACOB received a B.S. degree in physics from the California Institute of Technology, Pasadena, CA in 2001. He worked at MIT Lincoln Laboratory modeling radar cross sections for two years before entering graduate school at JILA and the University of Colorado-Boulder where he received a Ph.D. in physics in 2010 for his work on a quantum-limited detector of nanomechanical motion based on electron tunneling across

an atomic point contact. From 2010-2014 he was a Postdoctoral Associate at Yale University working on nanomechanical displacement measurements at the quantum limit using optical cavities. In 2014 he joined the Quantum Voltage Project at the National Institute of Standards and Technology (NIST), Boulder, CO, and has been working on development, characterization, and applications of the Josephson Arbitrary Waveform Synthesizer (JAWS), an ac Josephson voltage standard based on pulse-biased arrays of Josephson junctions. He received the IEEE Council on Superconductivity Van Duzer Prize in 2019.



PETER F. HOPKINS (Senior Member, IEEE) received the B.S. degree in engineering physics from the University of California, Berkeley in 1985, and the A.M. and Ph.D. degrees in physics from Harvard University, Cambridge, MA, in 1987 and 1990, respectively. In 2014, he joined the Superconductive Electronics Group, National Institute of Standards and Technology in Boulder, CO, USA. Since 2015, he has led the Flux Quantum Electronics Project,

researching the design, fabrication, and testing of high-speed superconductor electronics for energy-efficient computing, radio-frequency waveform synthesis, and scalable cryogenic quantum computing. Prior to joining NIST, he spent 19 years in the data storage industry where he productized hard-disk drives and solid-state drives for Quantum, Seagate, and Micron.



SAMUEL P. BENZ (Fellow, IEEE) was born in Dubuque, IA, on December 4, 1962. He received the B.A. degree (summa cum laude) in physics and math from Luther College, Decorah, IA, in 1985 and the M.A. and Ph.D. degrees in physics from Harvard University, Cambridge, MA, in 1987 and 1990, respectively. He was awarded an R.J. McElroy Fellowship (1985–1988) to work toward the Ph.D. degree.

In 1990, he joined the National Institute of Standards and Technology (NIST), Boulder, CO, as a NIST/NRC Postdoctoral Fellow and became a permanent Staff Member in January 1992. He has been the Project Leader of the Quantum Voltage Project at NIST since October 1999 and the Group Leader of the Superconductive Electronics Group since 2015. He has worked on a broad range of topics within the field of superconducting electronics, including Josephson junction array oscillators, single flux quantum logic, ac and dc Josephson voltage standards, Josephson waveform synthesis, and noise thermometry. He has over 320 publications and is the holder of five patents in the field of superconducting electronics. Dr. Benz is a Fellow of NIST, the American Physical Society (APS), and the IEEE. He is a member of Phi Beta Kappa and Sigma Pi Sigma. He has received three U.S. Department of Commerce Gold Medals for Distinguished Achievement, the 2016 IEEE Joseph F. Keithley Award, and the IEEE Council on Superconductivity Van Duzer Prize in 2006, 2016, and 2019.



DYLAN WILLIAMS (Life Fellow, IEEE) received a Ph.D. in Electrical Engineering from the University of California, Berkeley in 1986. He joined the Electromagnetic Fields Division of the National Institute of Standards and Technology in 1989 where he develops electrical waveform and microwave metrology. He has published over 140 technical papers and is a Fellow of the IEEE. He is the recipient of the Department of Commerce Bronze and Silver

Medals, the Astin Measurement Science Award, two Electrical Engineering Laboratory's Outstanding Paper Awards, three Automatic RF Techniques Group (ARFTG) Best Paper Awards, the ARFTG Automated Measurements Technology Award, the IEEE Morris E. Leeds Award, the European Microwave Prize and the 2013 IEEE Joseph F. Keithley Award. Dylan also served as Editor of the IEEE Transactions on Microwave Theory and Techniques from 2006 to 2010, as the Executive Editor of the IEEE Transactions on Terahertz Science and Technology, and as the 2017 President of the IEEE Microwave Theory and Techniques Society.